Wear 550-551 (2024) 205427

Contents lists available at ScienceDirect

Wear

journal homepage: www.elsevier.com/locate/wear

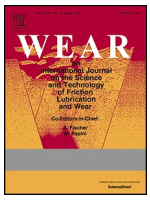

High temperature and high strain rate properties of brazed honeycomb liner material Haynes 214

Jonas Vogler [a], Rainer Völkl [a], Jieun Song [b], Vincent Fabian Viebranz [c], Jakob Huber [d], Hans-Jörg Bauer [b], Ewald Werner [d], Uwe Glatzel [a,*]

[a] Metals and Alloys, University of Bayreuth, Germany
[b] Institute of Thermal Turbomachinery, Karlsruhe Institute of Technology, Germany
[c] Institut für Werkstoffkunde (Materials Science), Leibniz University Hannover, Germany
[d] Institute of Materials Science, Technical University of Munich, Germany

ARTICLE INFO

Keywords:
Brazing
Haynes 214
Honeycomb
Nickel-base superalloys

ABSTRACT

Abradable honeycomb sealing systems are essential for gas turbine efficiency. Experimental data on the rubbing performance of Haynes 214 metal sheets brazed with the nickel-chromium-silicon filler metal BNi-5 is presented. The brazing layer in the double foiled honeycomb sections turned out to have a major impact on rubbing behavior. Damage on the rotor was analyzed with a large chamber scanning electron microscope and energy-dispersive X-ray spectroscopy. The results demonstrate a significant influence of the brazing process on the mechanical properties, especially after exposure to 1000 °C. A hard aluminum nitride phase formed in the brazed metal sheets can cause severe damage to the rotor.

1. Introduction

Labyrinth seals are crucial components in turbomachinery. A labyrinth seal consists of rotating seal fins and a stationary liner structure that enables a minimum clearance to reduce the leakage mass flow rate [1]. Rubbing events between the seal fins and liner structure are inevitable during engine operation [2–4]. As a requirement, damage to the seal fin must be prevented by limiting thermal and mechanical loads during rubbing.

The most significant wear mechanisms observed during high-speed rubbing include abrasive wear, wear from intense plastic deformations, melting of the friction partners, and adhesive material transfer [3,5,6]. Adhesive material transfer can lead to vibrations and larger wear particles. Plastic deformation can cause compaction or smearing of the pores, worsening wear resistance in subsequent rubbing processes and the degradation of sealing performance. Mechanical properties such as tensile strength, yield strength, and strain to failure, along with thermophysical properties like thermal conductivity and specific heat capacity, significantly impact rubbing properties [7–10].

Honeycomb liners are widely used for stationary liners. They are produced by corrugating metal sheets, spot-welding, and brazing the spot-welded structure onto a carrier plate. Due to capillary forces, the liquid braze filler alloy can flow up to the rubbing surface at the edges and in double foil sections of the corrugated and spot-welded metal sheets [11,12]. For Hastelloy X honeycomb liners brazed with BNi-5 Ulan kyzy et al. [11] detected the formation of hard and brittle NiSi- and $Ni_y(Mo, Cr)_xSi$-type silicides in the interdiffusion zones between the braze filler alloy and the metal sheets.

As shown in previous studies [12–14], the brazing layer can also influence the oxidation behavior of the composites. Huber et al. [15] investigated a layered composite of brazing metal and metal sheets employing numerical simulations. The simulations have shown that the volume ratio of the brittle phases strongly influences the mechanical behavior. However, little experimental work has been published on how the brazing layer affects mechanical and rubbing properties.

Therefore, this study compares microstructure and mechanical properties of Haynes 214 metal sheets before and after brazing with the braze filler alloy BNi-5. Operating conditions of a honeycomb sealing were simulated by exposing samples to air at 1000 °C for up to 150 h. Microstructural and mechanical investigations serve to identify critical parameters. The most important mechanical parameters are yield strength, tensile strength, and strain to failure. The most critical microstructural parameters are volume fractions, shape, and locations of the different brittle particles.

* Corresponding author.
E-mail address: uwe.glatzel@uni-bayreuth.de (U. Glatzel).

https://doi.org/10.1016/j.wear.2024.205427
Received 28 November 2023; Received in revised form 8 May 2024; Accepted 27 May 2024
Available online 28 May 2024

2. Experimental

The nickel-based superalloy Haynes 214 is commonly used in turbine seal honeycomb structures. Haynes 214 exhibits excellent oxidation resistance up to high temperatures due to the formation of a protective alumina scale. It can be age hardened at temperatures below 925 °C [16]. The nickel-based braze filler alloy BNi-5 (AMS4782) has a high liquidus temperature of approximately 1135 °C [17], making it well suited to join honeycomb structures with the base plates. The brazed honeycomb seals can withstand service temperatures up to 1100 °C [18]. The nominal compositions of Haynes 214 and the braze filler alloy BNi-5 are given in Table 1.

Elgiloy Specialty Metals supplied cold-rolled and at 1095 °C for 2 h annealed Haynes 214 sheets with 0.6 mm and 0.29 mm thickness. Two strips of the 0.29 mm thick sheet were brazed with 40 μm thick BNi-5 brazing foil by Listemann AG. Sandwich structure was selected to simulate double foil sections of the corrugated metal sheets in honeycomb sealing systems [12]. Brazing was conducted at a vacuum level of 10^{-1} Pa or better. The brazing temperature was 1170 °C with a holding time of 15 min. Subsequently, the samples were furnace cooled to 900 °C (~5 K/min) and then rapidly cooled to room temperature with a cooling rate of 20 K/min.

In order to simulate in-service conditions both, strips of 0.6 mm thick Haynes 214 and double-layer brazed Haynes 214 sandwiches, were annealed at 1000 °C for 75 h and 150 h in air followed by furnace cooling.

Mechanical testing of the brazed sandwich structures at room temperature was performed with a Zwick Z2.5 universal testing machine with the plane of the braze oriented parallel with respect to the tensile axis. The gauge length of the Zwick Z2.5 miniature specimens was 5 mm with a width of 0.9 mm, hence, a crosshead speed of 0.05 mm/s results in an engineering strain rate of approximately 10^{-2} s^{-1}. To determine mechanical parameters at high strain rates of up to 50 s^{-1} and high temperatures of up to 1100 °C, the servo-hydraulic tensile testing machine Gleeble 3500 was used. The gauge length of the Gleeble 3500 specimens was 8 mm with a width of 5 mm. Samples were produced by electron discharge machining. Strain was measured with a video extensometer.

The mechanical in-service performances of the brazed metal sheets were investigated with a rubbing test rig at the Karlsruhe Institute of Technology. A schematic drawing of the test setup and a photograph of an ongoing rubbing test are shown in Fig. 1.

The metal sheets were mounted to a foil holder and secured with two screws as shown in Fig. 1. A stepper motor-driven traversing system enables the radial incursion of the metal sheets into the seal fin to a defined incursion depth of 1 mm at an incursion rate of 0.25 mm/s. The rotor material was Inconel 718 (Table 1). The rotor fin had a thickness of 0.6 mm. The metal sheets were 15 mm high, and the contact surface A_C was 12 mm × 0.6 mm. The metal sheets were positioned parallel to the rotor fin to simulate contact between double foil segments of honeycomb sealings and the rotor fin. Rubbing tests were performed with a fin tip speed of 110 m/s. The resulting contact forces, temperatures, and weight losses were measured. The coefficient of friction was calculated by dividing the mean frictional force by the mean normal force. The test rig is described in detail by Pychynski et al. [20] and Hühn et al. [21].

Microstructure studies were carried out using scanning electron microscopy (SEM). Element distribution analysis was performed by energy-dispersive X-ray spectroscopy (EDS) and wavelength-dispersive X-ray spectrometry (WDS). Non-destructive surface analysis of the rotor after the rubbing tests was carried out at the Leibniz University Hannover in a large chamber scanning electron microscope (LC-SEM).

3. Results and discussions

3.1. Microstructure

The as-delivered Haynes 214 single metal sheets have an equiaxed grain structure with an average grain size of 30 μm. Quantitative measurements of carbon using WDS revealed a carbon content of 1.3 wt% in the alloy. The microstructures of the Haynes 214 single metal sheets in the as-delivered condition and after exposure to 1000 °C for 75 h and 150 h are given in Fig. 2.

During annealing at 1000 °C precipitates with a diameter smaller than 5 μm form at grain boundaries. EDS measurements indicate that the precipitates are chromium carbides. Such a formation of carbides is expected when Haynes 214 is exposed to temperatures below its solution heat-treatment temperature of 1095 °C [16].

Fig. 3 shows the microstructures of an as-brazed sample, after exposure to 1000 °C for 75 h and after exposure to 1000 °C for 150 h. The brazing process of 15 min at 1170 °C results in considerable growth of the average grain size from 30 μm to 330 μm.

The width of the silicon-rich diffusion-affected zone is approximately 50 μm in the as-brazed condition [22]. Furthermore, chromium carbides were detected in the center of the joint region and along grain boundaries. After exposure to 1000 °C for 75 h, the chromium carbides in the center of the joint have almost completely dissolved. Instead, formation of aluminum nitride precipitates is observed (black particles in Fig. 3b and c). The volume fraction of aluminum nitride precipitates increases with exposure time and reaches a volume fraction of about 1.5 % after 150 h at 1000 °C (Fig. 3c). EDS mappings of the brazed sample annealed for 150 h revealing the presence of the aluminum nitride precipitates can be found in Fig. 4. The width of the silicon-rich diffusion-affected zone with more than 1 wt % silicon in the alloy increased to approximately 150 μm after annealing at 1000 °C for 150 h.

To further study the formation of the aluminum nitrides in the brazed and annealed samples, the oxide scale was analyzed, and the results are shown in Fig. 5. The chemical compositions of the points marked in Fig. 5 are listed in Table 2.

From Fig. 5 and Table 2 it is evident that a chromium oxide scale has formed at the surface of the brazed and annealed sample (spots 5 + 6). Beneath the chromium oxide scale, there are aluminum oxide precipitates that have formed due to internal oxidation (spots 3 + 4). Already at a depth of approximately 40 μm below the oxide layer, aluminum nitride precipitates can be observed (spots 1 + 2).

Haynes 214 is highly resistant to oxidation at elevated temperatures, primarily attributed to the formation of a protective Al_2O_3 scale. However, annealing the brazed samples at 1000 °C results in the formation of a chromium oxide scale. The brazing process (oxygen partial pressure, temperature, and evaporation) and the change in composition due to elemental diffusion from the braze filler alloy into the base material can lead to this change in oxide scale formation. Unlike a typical aluminum oxide scale, the chromium oxide scale exhibits permeability for nitrogen. Consequently, nitrogen diffuses into the brazed samples, leading to an occurrence of internal aluminum nitrides. Nitride formation beneath a chromia scale has been previously documented by Jalowicka et al. [23], Michalik et al. [24] and Zheng et al. [25]. The formation of

Table 1
Nominal chemical composition (wt%) of the Haynes 214 metal sheets, the Inconel 718 rotor, and the brazing filler alloy BNi-5 used in this study [16,17,19].

Element in wt%	Ni	Cr	Si	Al	Fe	Nb	Mo	Ti	Co
Haynes 214	75 (bal.)	16	<0.2	4.5	3	<0.2	<0.5	<0.5	<2
Inconel 718	50–55	17–21	<0.35	0.2–0.8	17 (bal.)	4.8–5.5	2.8–3.3	0.7–1.2	<1
BNi-5	71 (bal.)	19	10						

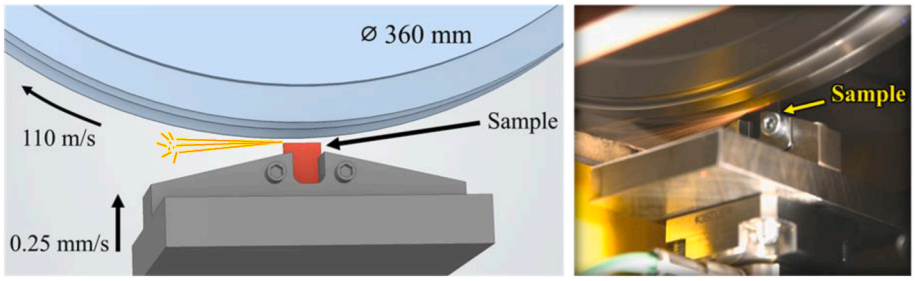

Fig. 1. Rubbing test rig featuring the metal sheet sample highlighted in red. The photograph on the right captures the ongoing experiment. Sparks can be observed, emanating from the surface. Heat is causing the metal sheet to glow in the contact area. (For interpretation of the references to color in this figure legend, the reader is referred to the Web version of this article.)

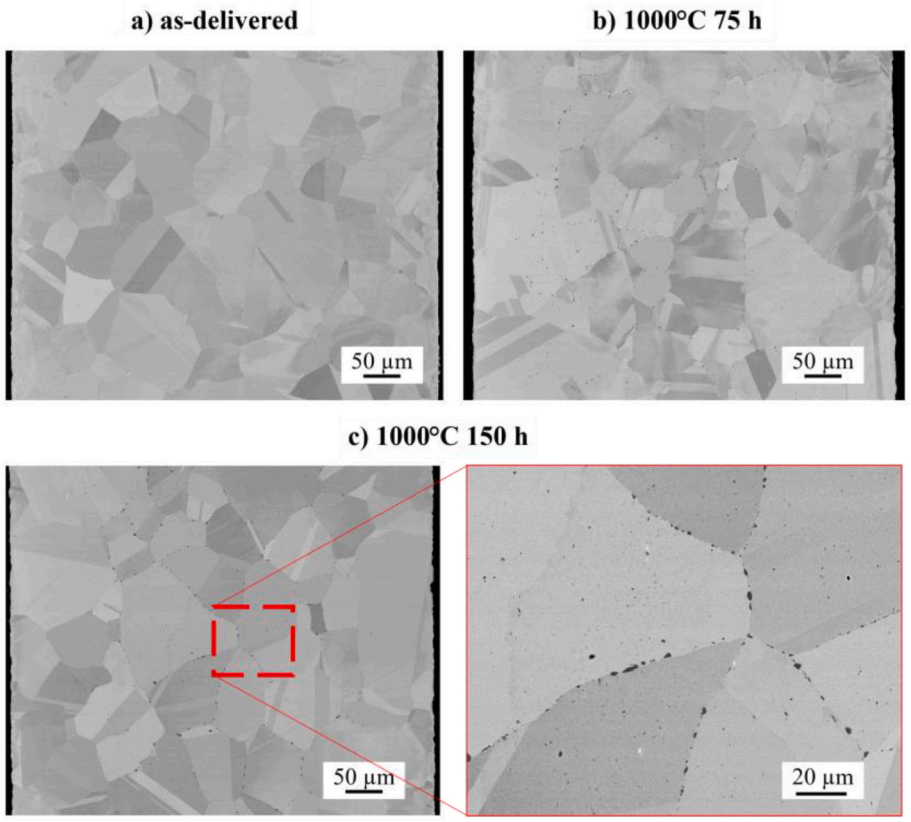

Fig. 2. Haynes 214 single metal sheet microstructures a) in the as-delivered condition, b) after 75 h at 1000 °C, and c) after 150 h at 1000 °C.

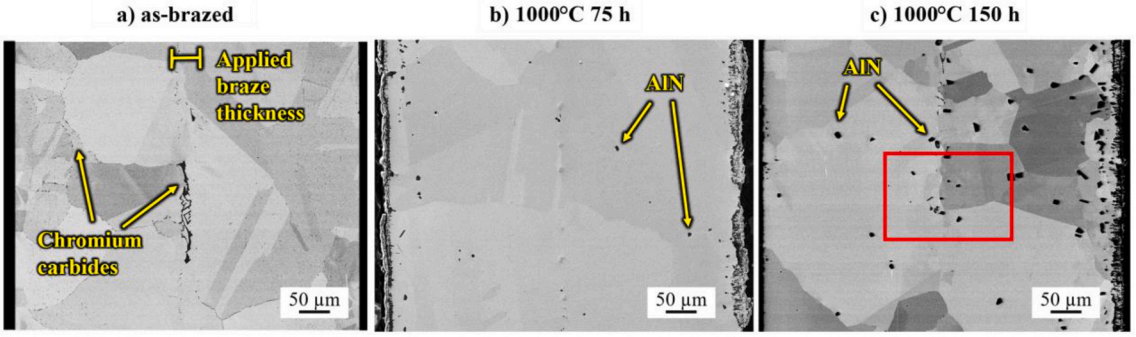

Fig. 3. Microstructure of the brazed Haynes 214 samples a) in the as-brazed condition, b) after 75 h at 1000 °C, and c) after 150 h at 1000 °C. The area marked in c) is shown in detail in Fig. 4.

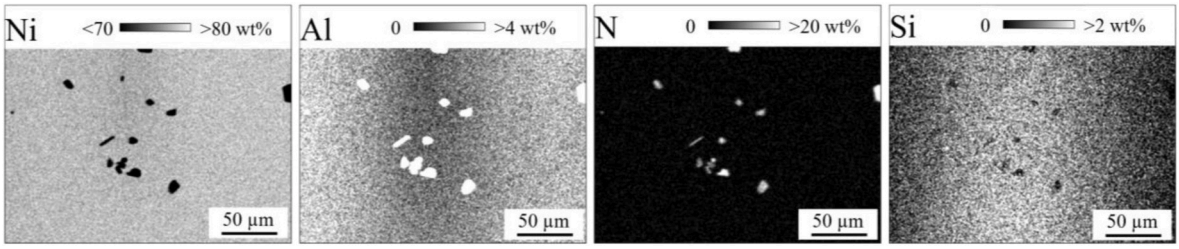

Fig. 4. Quantitative EDS mapping in the middle of the brazing joint after 150 h at 1000 °C (area marked in Fig. 3c).

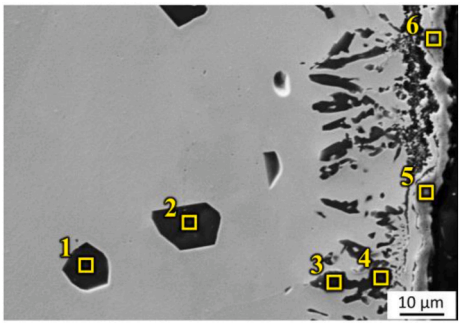

Fig. 5. Microstructure at the surface of the brazed Haynes 214 samples after 150 h at 1000 °C.

precipitates and accelerated oxidation in Haynes 214 honeycomb liners at 1100 °C could also be found by Sporer et al. [12]. They explained the accelerated oxidation damage by diffusion of elements from the braze filler alloy into the base metal.

3.2. Tensile properties

Fig. 6 shows representative stress-strain curves for the 0.6 mm thick Haynes 214 single metal sheets and BNi-5 brazed ~0.6 mm thick double-layer sandwiches of Haynes 214 in the as-brazed condition and after exposure to 1000 °C. The mean values of the ultimate tensile strength and the strain to failure of five tests are listed in Table 3.

The yield strength and the ultimate tensile strength of the Haynes 214 samples are increased after exposure to 1000 °C. The higher tensile strength and reduced strain to failure after annealing can be attributed to the precipitation of chromium carbides, as observed in Fig. 2.

When comparing the stress-strain curves of the Haynes 214 samples (Fig. 6a) with those of the as-brazed sample (Fig. 6b), it can be observed that the strain to failure is strongly reduced from 36 % to 18 %. The yield strength and the ultimate tensile strength decrease after annealing the brazed samples at 1000 °C. The difference in the mechanical properties between the 75 h and the 150 h exposure at 1000 °C is marginal. The chromium carbide precipitates at the brazing centerline observed in Fig. 3 cause stress concentrations in the brazed metal sheets. Thereby strain to failure (ductility) is reduced. The dissolution of the chromium carbides after annealing at 1000 °C leads to the increase in strain to failure and a reduction in tensile strength for the brazed samples (Fig. 6b).

Fig. 7 shows tensile test results at high strain rates of 1 s^{-1} and 50 s^{-1} and at high temperatures. Ultimate tensile strength and the strain to failure at a strain rate of 1 s^{-1} are similar to tensile tests with a strain rate of 10^{-2} s^{-1}. The ultimate tensile strengths of the Haynes 214 samples at

Table 2
Compositions (wt%) of the spots marked in Fig. 5.

Spot	Element							
	C	N	O	Al	Cr	Fe	Ni	Deduced phase
1 + 2	3.4	**25.6**	0.0	**69.1**	0.3	0.1	1.5	Aluminum nitride (AlN) ≙ 66 wt% Al, 34 wt% N
3 + 4	1.9	0.8	**39.7**	**46.1**	2.6	0.5	8.4	Aluminum oxide (Al_2O_3) ≙ 53 wt% Al, 47 wt% O
5 + 6	1.8	0.5	**32.9**	0.7	**61.0**	0.2	2.9	Chromium oxide (Cr_2O_3) ≙ 68 wt% Cr, 32 wt% O

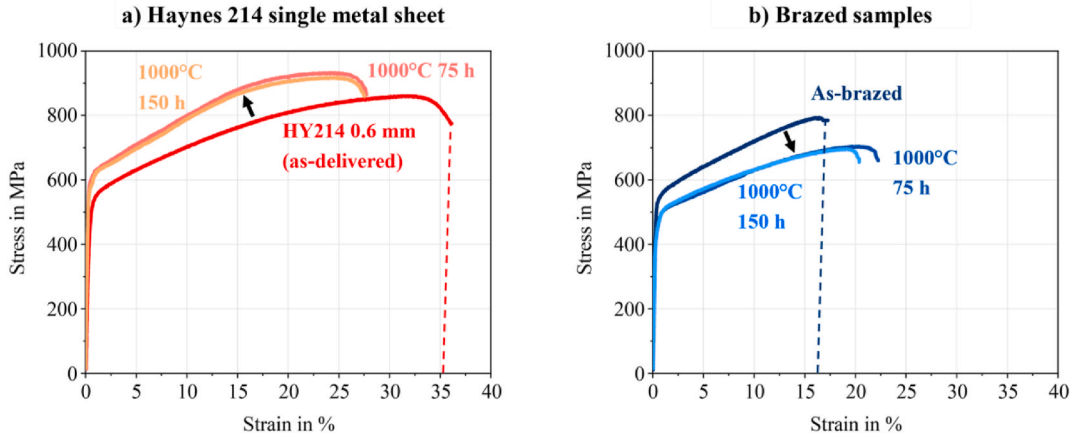

Fig. 6. Engineering stress-strain plots of a) Haynes 214 samples and b) brazed samples. Comparison between samples without and after exposure to 1000 °C for 75 h and 150 h.

Table 3
Tensile properties of Haynes 214 (HY214) and brazed metal sheets at room temperature in the as-delivered condition and after exposure to 1000 °C for 75 h and 150 h.

	As-delivered		1000 °C 75 h		1000 °C 150 h	
	Haynes 214	Brazed	Haynes 214	Brazed	Haynes 214	Brazed
Ultimate tensile strength	850 MPa	795 MPa	935 MPa	715 MPa	915 MPa	685 MPa
Strain to failure	36 %	18 %	28 %	24 %	28 %	22 %

a strain rate of 50 s^{-1} are higher compared to the lower strain rate tensile tests. This aligns with the research by Wang et al. [26], indicating a rise in the yield strength of a Ni-based superalloy as the strain rate increases, particularly surpassing 10 s^{-1}. Additionally, their findings suggest a reduction in the strain to failure as the strain rate rises. This can also be seen for the high strain rate tensile tests in Fig. 7b. However, an exception arises with the Haynes 214 metal sheets at room temperatures, as they exhibit a consistent strain to failure of around 35 % regardless of the applied strain rate. At 1100 °C and 50 s^{-1}, the brazed sample exhibits an exceptionally low elongation. This is attributed to a defect in the brazed metal sheet, such as a pore or accumulation of chromium carbides.

3.3. Rubbing test results

Fig. 8 shows the coefficient of friction and the weight loss of various sheet samples after rubbing. The friction coefficient increases slightly after brazing. Moreover, the coefficient of friction in the brazed double-layer sandwich samples further increases with longer annealing at 1000 °C.

The weight loss of as-brazed sandwiches is smaller than the weight loss of Haynes 214 single metal sheets. Weight loss of the annealed samples increases with increasing annealing time. The measurement scatter in Fig. 8 is explained by the scatter of final incursion depth, incursion rate, and resulting rub duration [20]. Nevertheless, the higher weight loss of the brazed and annealed sandwich samples indicates increased abrasive wear. Fig. 9 illustrates the damage observed in the brazed and rubbed samples. In the as-brazed condition, cracks along the brazing joint line are clearly visible.

The "mushrooming" of the sandwiches is similar to worn honeycomb liners after seal fin rubbing, as shown by Ulan kyzy et al. [27] and Sporer and Shiembob [12]. High contact zone temperatures of around 800 °C [20] reduce the yield strength of the material (Fig. 7). The softened material in the contact region is then squeezed outwards as the incursion progresses [9].

To describe the degree of plastic deformation, Xue et al. [28] and Ulan Kyzy et al. [27] determine the mushroom crown volume. The mushroom crown volume V_P is calculated by multiplying the area on both sides with the length of the sample (12 mm). The converted images and the corresponding mushroom crown volume V_p are shown in Fig. 10.

The mushroom crown volume of the as-brazed sample is up to four times larger than that of the brazed and annealed samples. Additionally, cracks in the brazed joint area of the as-brazed sample are detected after rubbing (Figs. 9a and 10a). Particles of the brittle chromium-rich phase along the braze centerline of the as-brazed sandwich provoke cracking along the centerline. Therefore, the brazed sandwich splits during the rubbing test and plastic deformation of the ductile sandwich halves result in a mushroom crown volume increase of more than 300 %.

The rubbing properties and the images of the brazed and annealed samples show a change in the deformation mechanism from plastic deformation to abrasive wear. The differences in the rubbing properties suggest that the location of the brittle phases in the samples significantly influences the deformation mechanism. While the brittle chromium-rich phase at the braze centerline of the as-brazed samples promotes splitting of the brazed samples, the evenly distributed aluminum nitride precipitates in the brazed and annealed samples (Fig. 3) cause an increase in abrasive wear. Therefore, the mushroom crown volume of the annealed samples is strongly decreased (Fig. 10). The increase in abrasive wear of the brazed and annealed samples is also consistent with the increased weight loss after the rubbing test (Fig. 8).

The fin of the rotor made of Inconel 718 is examined in a large chamber SEM. The fin was sequentially employed for rubbing tests with Haynes 214 metal sheets, followed by as-brazed samples, and brazed annealed samples. Fig. 11 shows BSE images of the surface analysis.

At the rotor's surface, cracks in the direction of motion of the rotor are visible (Fig. 11a I). A corresponding EDS line scan perpendicular to the direction of motion of the rotor as indicated in Fig. 11b is given in Fig. 12. The dark grey areas (Fig. 11a II) have oxygen contents of more than 20 wt%. Together with increased aluminum and chromium concentrations at the same area, the presence of aluminum oxide and chromium oxide or mixed oxides is obvious. Chromium and aluminum are depleted at the edges of the oxygen-rich zone, whereas a nickel concentration jump is measured.

Regions with higher aluminum content and lower iron content confirm that Haynes 214 is transferred from the metal sheets to the Inconel 718 rotor surface. Overall, no significant damage to the rotor is observed through non-destructive testing using a large chamber SEM. Areas with material transfer and minor cracks in the transferred material are detected.

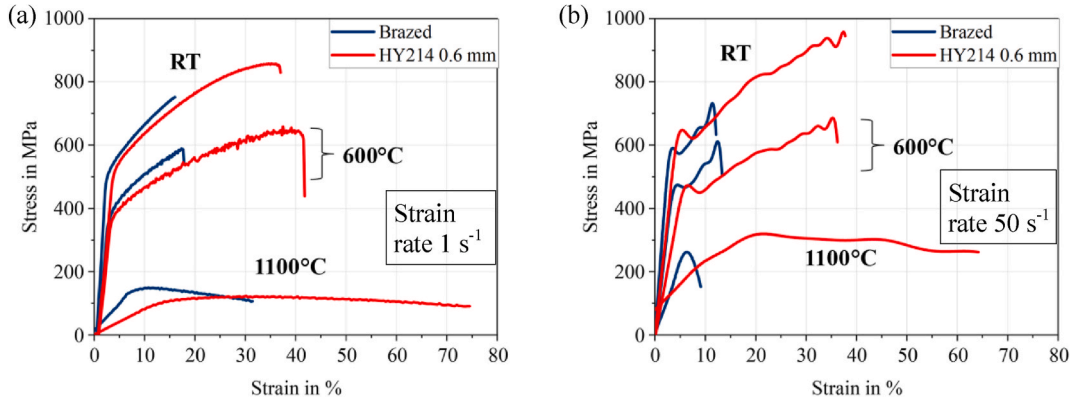

Fig. 7. Engineering stress - engineering strain plots at high strain rates of the Haynes 214 samples and the brazed samples at room temperature, 600 °C, and 1100 °C with a strain rate of 1 s^{-1} (a) and 50 s^{-1} (b).

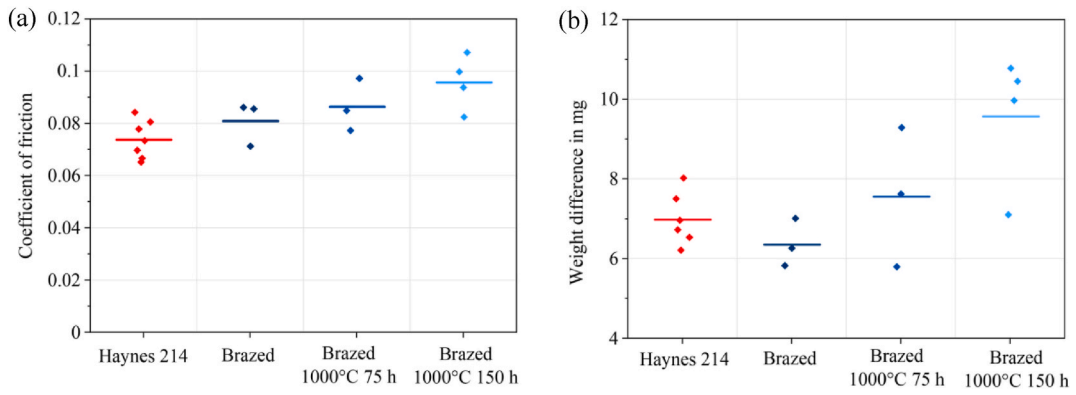

Fig. 8. Coefficient of friction (a) and weight loss (b) during rubbing of Haynes 214 single metal sheet and double-layer sandwiches as-brazed and annealed respectively. Horizontal lines indicate mean values.

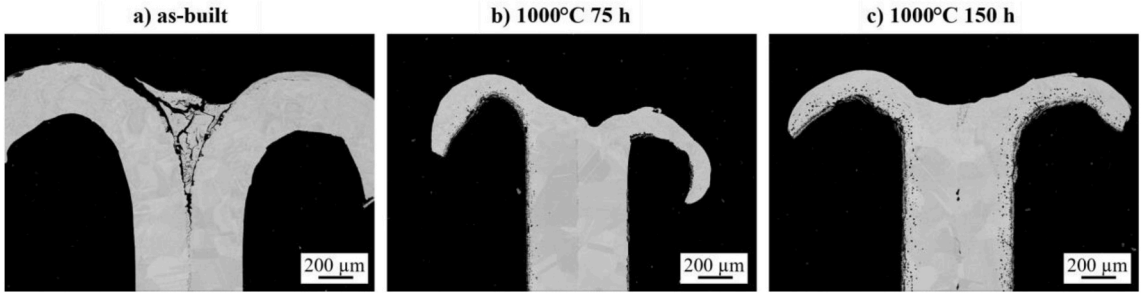

Fig. 9. Backscattered electron image of the rubbed double-layer sandwiches in the as-brazed condition and after annealing to 1000 °C for 75 h and 150 h.

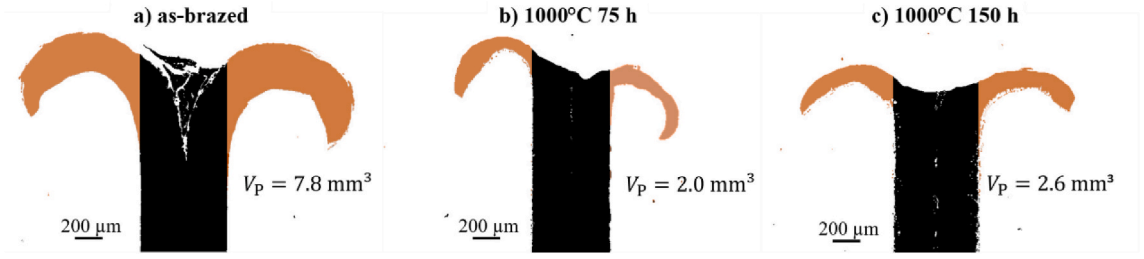

Fig. 10. Binary image from the ImageJ software used to measure the mushroom crown volume of the brazed samples. The brown-colored areas indicate the measured mushroom crown area. (For interpretation of the references to color in this figure legend, the reader is referred to the Web version of this article.)

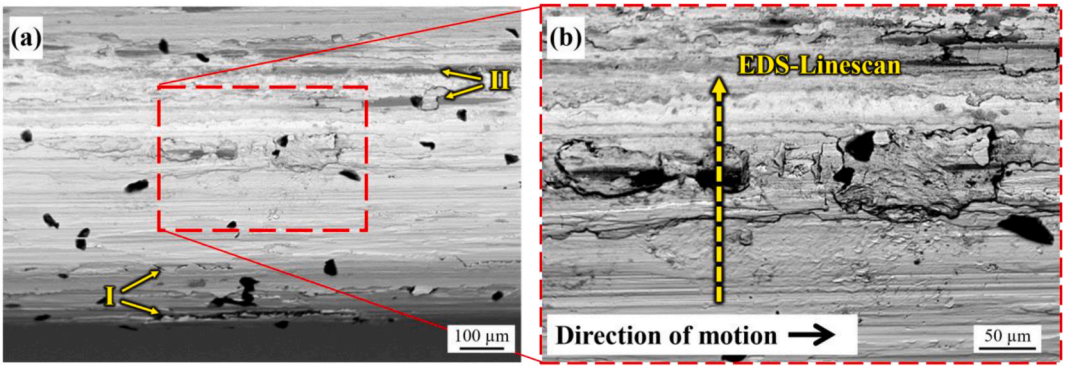

Fig. 11. BSE image of the Inconel 718 rotor fin after rubbing tests with brazed Haynes 214 metal sheets.

Avoiding adhesive material transfer is essential since the material transfer leads to an increase in the temperature of the seal fin tip [4]. The higher temperatures can result in an accelerated wear process and the formation of radial cracks in the rotor fin due to tensile stress caused by contact heat [29,30]. Therefore, the rubbing tests suggest that the samples in the as-brazed condition exhibit better rubbing properties

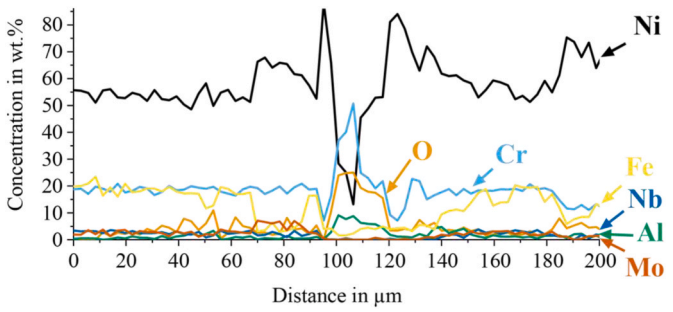

Fig. 12. EDS line scan of the Inconel 718 rotor after rubbing perpendicular to rotor motion direction.

than the brazed and annealed samples. The brazing material within the gap of the double wall segments in the honeycomb sealing system increases the area subjected to rubbing, consequently increasing the stress on the rotor fin.

4. Summary

In this work, the influence of the braze filler alloy BNi-5 on the microstructural, mechanical, and rubbing properties of brazed Haynes 214 nickel-based superalloy metal sheets was studied. The differences between the brazed and the brazed and annealed samples are summarized as follows:

After brazing:

- Chromium carbides localized in the joint region and at the grain boundaries.
- 50 µm silicon-rich diffusion-affected zone.
- Strain to failure decreases from 36 % to 18 %.

After brazing and annealing at 1000 °C for 150 h:

- Chromium oxide scale forms on the surface of the brazed samples, while an aluminum oxide scale develops on the Haynes 214 single metal sheets.
- Chromium carbides dissolve and aluminum nitrides are formed.
- 150 µm silicon-rich diffusion-affected zone.

The rubbing properties are significantly affected, with the brazed samples exhibiting higher coefficients of friction against an Inconel 718 rotor. Inspection of the rotor fin's surface reveals adhesive material transfer, cracks, and oxide formation. The increased wear in the brazed and annealed samples is attributed to the presence of hard aluminum nitrides and the even distribution of chromium carbides, which are no longer concentrated along the brazing center line as they were in the as-brazed condition. Hence, it is imperative to eliminate any excess braze metal alloy within the double foil segments of honeycomb sealing systems to effectively minimize thermal and mechanical stresses on the rotor fin. To enhance oxidation behavior and prevent aluminum nitride formation, it is advisable to apply a protective aluminum coating or to utilize base materials with elevated aluminum content.

CRediT authorship contribution statement

Jonas Vogler: Writing – review & editing, Writing – original draft, Investigation. **Rainer Völkl:** Writing – review & editing, Supervision, Funding acquisition. **Jieun Song:** Writing – review & editing, Investigation. **Vincent Fabian Viebranz:** Investigation. **Jakob Huber:** Writing – review & editing, Investigation. **Hans-Jörg Bauer:** Supervision, Funding acquisition. **Ewald Werner:** Writing – review & editing, Supervision, Funding acquisition. **Uwe Glatzel:** Writing – review & editing, Supervision, Funding acquisition.

Declaration of competing interest

The authors declare that they have no known competing financial interests or personal relationships that could have appeared to influence the work reported in this paper.

Data availability

Data will be made available on request.

Acknowledgements

This work was supported by the DFG (Deutsche Forschungsgemeinschaft) in the context of the research projects GL 181/40-3, WE 2351/14-3, and BA 2848/5-3. We would like to express our sincere gratitude to Dr.-Ing. H.-W. Höppel and M. Sc. P. M. Pohl from the Department of Materials Science and Engineering, Institute I: General Materials Properties, Friedrich-Alexander-Universität Erlangen-Nürnberg for their contribution in conducting non-destructive examinations of the rotor using the Large Chamber Scanning Electron Microscope in previous studies.

References

[1] H.L. Stocker, D.M. Cox, G.F. Holle, Aerodynamic Performance of Conventional and Advanced Design Labyrinth Seals with Solid-Smooth Abradable, and Honeycomb Lands, NASA, 1977. CR-135307 (EDR 9339).
[2] S. Lattime, B. Steinetz, Turbine Engine Clearance Control Systems: Current Practices and Future Directions, National Aeronautics and Space Administration, Glenn Research Center, 2002. Report No. NASA/TM-2002-211794.
[3] R.C. Bill, L.P. Ludwig, Wear of seal materials used in aircraft propulsion systems, Wear 59 (1980) 165–189, https://doi.org/10.1016/0043-1648(80)90277-X.
[4] A. Rossmann, Reibverschleiß, Anstreifen und Spalthaltung, Labyrinthdichtungen, Bürstendichtungen, Containment, Feuer und Explosionen, first. Aufl., Turbo Consult, Karlsfeld, 2000.
[5] W.H. Xue, S.Y. Gao, D.L. Duan, Y. Liu, S. Li, Material transfer behaviour between a Ti6Al4V blade and an aluminium hexagonal boron nitride abradable coating during high-speed rubbing, Wear 322–323 (2015) 76–90, https://doi.org/10.1016/j.wear.2014.10.001.
[6] M.O. Borel, A.R. Nicoll, H.W. Schläpfer, R.K. Schmid, The wear mechanisms occurring in abradable seals of gas turbines, Surf. Coating. Technol. 39–40 (1989) 117–126, https://doi.org/10.1016/0257-8972(89)90046-7.
[7] W.D. Marscher, A phenomenological model of abradable wear in high performance turbomachinery, Wear 59 (1980) 191–211, https://doi.org/10.1016/0043-1648(80)90278-1.
[8] S. Gao, W. Xue, D. Duan, S. Li, H. Zheng, Effect of thermal–physical properties on the abradability of seal coating under high-speed rubbing condition, Wear 394–395 (2018) 20–29, https://doi.org/10.1016/j.wear.2017.09.006.
[9] F. Ghasripoor, N.A. Turnquist, M. Kowalczyk, B. Couture, Wear prediction of strip seals through conductance, ASME turbo expo 2004: power for land, Sea, and Air (2004) 331–337, https://doi.org/10.1115/GT2004-53297.
[10] H. Wang, Criteria for analysis of abradable coatings, Surf. Coating. Technol. 79 (1996) 71–75, https://doi.org/10.1016/0257-8972(95)02443-3.
[11] S. Ulan kyzy, R. Völkl, O. Munz, T. Fischer, U. Glatzel, The effect of brazing on microstructure of honeycomb liner material hastelloy X, J. Of materi, Eng and Perform 28 (2019) 1909–1913, https://doi.org/10.1007/s11665-019-03910-w.
[12] D.R. Sporer, L.T. Shiembob, in: Alloy Selection for Honeycomb Gas Path Seal Systems, vol. 4, Turbo Expo, 2004, pp. 763–774.
[13] N.J. Simms, R. Newton, J.F. Norton, A. Encinas-Oropesa, J.E. Oakey, J.R. Nicholls, J. Wilber, Degradation of Fe–Cr–Al–RE and Ni–Cr–Al–RE foils in air and combustion gas atmospheres, Mater. A. T. High. Temp. 20 (2003) 439–451, https://doi.org/10.1179/mht.2003.051.
[14] D.J. Potter, Y.W. Chai, G.J. Tatlock, Improvements in honeycomb abradable seals, Mater. A. T. High. Temp. 26 (2009) 127–135, https://doi.org/10.3184/096034009X464302.
[15] J. Huber, J. Vogler, E. Werner, Multiscale modeling of the mechanical behavior of brazed Ni-based superalloy sheet metals, Continuum Mech. Therm. 35 (2023) 211–229, https://doi.org/10.1007/s00161-022-01172-x.
[16] Haynes International, Data Sheet Haynes 214, 2021.
[17] The Prince & Izant Company, Data Sheet AMS 4782 (BNi-5), 2021.
[18] Dieter Sporer, Dientje Fortuna, Selecting materials for brazing a honeycomb in turbine engines, Weld. J. (2014) 2014.
[19] Special Metals Corporation, Data Sheet INCONEL® Alloy 718, 2007.
[20] T. Pychynski, C. Höfler, H.-J. Bauer, Experimental study on the friction contact between a labyrinth seal fin and a honeycomb stator, J. Eng. Gas Turbines Power 138 (2016) 062501, https://doi.org/10.1115/1.4031791.
[21] L. Hühn, O. Munz, C. Schwitzke, H.-J. Bauer, Experimental investigation on the rubbing process of labyrinth seals considering the material combination, in:

Volume 10A: Structures and Dynamics, Virtual, Online, American Society of Mechanical Engineers, 2020.
[22] J. Vogler, J. Song, J. Huber, R. Völkl, U. Glatzel, Mechanical and microstructural properties of brazed honeycomb liner material Haynes 214, in: E.A. Ott, J. Andersson, C. Sudbrack, Z. Bi, K. Bockenstedt, I. Dempster, M. Fahrmann, P. Jablonski, M. Kirka, X. Liu, D. Nagahama, T. Smith, M. Stockinger, A. Wessman (Eds.), Proceedings of the 10th International Symposium on Superalloy 718 and Derivatives, Springer Nature Switzerland, Cham, 2023, pp. 445–452.
[23] A. Jalowicka, W. Nowak, D.J. Young, V. Nischwitz, D. Naumenko, W. J. Quadakkers, Boron depletion in a nickel base superalloy induced by high temperature oxidation, Oxid Met 83 (2015) 393–413, https://doi.org/10.1007/s11085-015-9529-4.
[24] M. Michalik, S.L. Tobing, M. Hänsel, V. Shemet, W.J. Quadakkers, D.J. Young, Effects of water vapour on the high temperature nitridation of chromium, Mater. Corros. 65 (2014) 260–266, https://doi.org/10.1002/maco.201307160.
[25] X.G. Zheng, D.J. Young, High-temperature corrosion of Cr_2O_3-forming alloys in CO-CO_2-N_2 atmospheres, Oxid Met 42 (1994) 163–190, https://doi.org/10.1007/BF01052021.
[26] L. Wang, Y. Liu, X. Song, J. Jin, J. Du, B. Zhang, Study on the strain rate sensitivity of a Ni-based superalloy, in: F. Marquis (Ed.), Proceedings of the 8th Pacific Rim International Congress on Advanced Materials and Processing, Springer, Cham, 2016, pp. 469–474.
[27] S. Ulan kyzy, Werkstoffeigenschaften und Anstreifverhalten von Nickelbasis-Superlegierungen verwendet für Honigwabeneinlaufbeläge, 2020. PhD-thesis, Düren.
[28] W. Xue, S. Gao, D. Duan, H. Zheng, S. Li, Investigation and simulation of the shear lip phenomenon observed in a high-speed abradable seal for use in aero-engines, Wear 386 (387) (2017) 195–203, https://doi.org/10.1016/j.wear.2017.06.019.
[29] T. Pychynski, K. Dullenkopf, H.-J. Bauer, Theoretical study on the origin of radial cracks in labyrinth seal fins due to rubbing, in: Volume 7A: Structures and Dynamics, American Society of Mechanical Engineers, San Antonio, Texas, USA, 2013.
[30] L. Hühn, F. Rieger, F. Bleier, C. Schwitzke, H.-J. Bauer, T. Behnisch, Extensive investigations on radial crack formation in labyrinth seals of aircraft engines, Deutscher Luft- und Raumfahrtkongress (2018), https://doi.org/10.5445/IR/1000093322.